Analytical Methods

ROYAL SOCIETY OF CHEMISTRY

PAPER

View Article Online
View Journal | View Issue



Cite this: *Anal. Methods*, 2022, **14**, 843

# A novel electrochemical sandwich-like immunosensor based on carboxyl $Ti_3C_2T_x$ MXene and rhodamine b/gold/reduced graphene oxide for *Listeria monocytogenes*

Huimin Niu,†[ab] Shumei Cai,†[ab] Xueke Liu,†[ab] Xiaoming Huang,[ab] Juan Chen,[ab] Shuiliang Wang *[ab] and Shenghang Zhang *[ab]

Received 30th November 2021
Accepted 20th January 2022

DOI: 10.1039/d1ay02029c

rsc.li/methods

*Listeria monocytogenes* (LM) is one of the most common food-borne pathogens and can induce a series of diseases with a high mortality rate to humans; hence, it is very necessary to develop a highly sensitive method for LM detection. Based on this need, a new sandwich-like electrochemical immunosensing platform was developed herein by preparing carboxyl $Ti_3C_2T_x$ MXene (C-$Ti_3C_2T_x$ MXene) as the sensing platform and rhodamine b/gold/reduced graphene oxide (RhB/Au/RGO) as the signal amplifier. The high conductivity and large surface area of C-$Ti_3C_2T_x$ MXene make it a desirable nanomaterial to fix the primary antibody of LM (PAb), while the prepared Au/RGO/RhB nanohybrid is dedicated to assembling the secondary antibody (SAb) of LM, offering an amplified response signal. Through the use of RhB molecule as the signal probe, the experiments showed that the peak currents of RhB increase along with an increase in the concentration of LM from 10 to $10^5$ CFU $mL^{-1}$, and an extremely low limit of detection (2 CFU $mL^{-1}$) was obtained on the basis of the proposed immunosensing platform after optimizing various conditions. Hence, it is confirmed that the developed sandwich-like immunosensor based on C-$Ti_3C_2T_x$ MXene and RhB/Au/Gr has great application in the detection of LM and other analytes.



## 1. Introduction

As one of the most common food-borne pathogens, *Listeria monocytogenes* (LM) can induce various serious diseases (*e.g.* meningitis, febrile gastroenteritis, abortion and septicemia) to human health.[1–3] LM can survive easily in a series of foods including water, cheese, milk, meats and raw vegetables.[4,5] In the USA, a zero-tolerance policy was formed for the presence of LM in food; in Canada, only 100 CFU $g^{-1}$ was allowed.[6,7] Consequently, developing effective methods to achieve sensitive detection of LM is considerably important. Up to now, several conventional methods (*e.g.* dynamic light scattering immunoassay, lateral-flow enzyme immunoconcentration, enzyme-linked immunosorbent assay and quartz crystal microbalance immunosensors) have been developed for LM detection.[4,8–11] There is no doubt that these methods are very important in detecting LM, but they suffer from drawbacks which include time-consuming process, expensive equipment or complex operation. Compared to the general methods, electrochemical technology has many incomparable merits since it is very simple, low-cost, easy to operate, and time-saving.[12] In the last few years, there have been some interesting electrochemical sensing methods proposed to detect LM,[13–15] while developing a sensing platform with higher performance is still a major challenge.

Resulting from the superior signal amplification feature, which causes improvement in sensitivity, the sandwich-like electrochemical immunosensing strategy has aroused considerable attention in recent years.[16–18] As one of the crucial factors, designing suitable materials as sensing platform, which is dedicated to immobilize antibodies coupled with improved electron transfer, is of great significance.[19,20] MXenes, known as transition metal carbides/carbonitrides, are an emerging representative 2D nanomaterials in recent years due to their excellent properties.[21–23] MXenes were discovered *via* exfoliating the "A" laminar component from the MAX phase, which represents the corresponding components in compounds, where "M" reflects the transition metal, "A" refers to the elements in group IIIA/IVA, and "X" is assigned to C/N.[24–29] The high electrical conductivity and large surface area of MXenes make MXenes-based nanomaterials have important applications in many fields.[30–32] In fact, presently MXenes have been applied widely in energy storage and conversion, sensors and biomedicine,[33–36] but there are only a few reports focused on their application in electrochemical immunosensors.

[a]*Fujian Key Laboratory of Aptamers Technology, Affiliated Dongfang Hospital of School of Medicine, Xiamen University, Fuzhou, Fujian 350025, PR China. E-mail: fzzyyzsh@126.com; shuiliang.wang@xmu.edu.cn*

[b]*Department of Clinical Laboratory Medicine, Fuzhou General Clinical Medical School (the 900th Hospital), Fujian Medical University, Fuzhou, Fujian 350025, PR China*

† These authors contributed equally to this work.

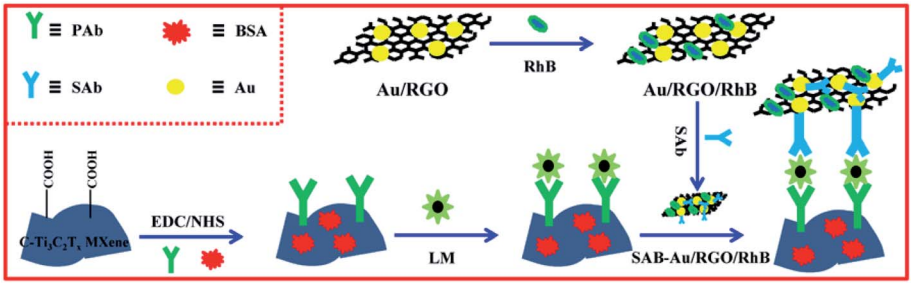


Scheme 1 Illustrations for constructing the sandwich-like immunosensor of LM based on C-$Ti_3C_2T_x$ MXene and RhB/Au/RGO.

Another key factor in the sandwich-like immunosensor is designing a desirable nanostructure as signal amplifier, which is also very important for improving sensing sensitivity. As another star material, reduced graphene oxide (RGO) possesses many excellent advantages such as large surface area, high electrical conductivity and chemical stability; moreover, RGO can easily be functionalized.[37–40] Presently, various RGO-based nanostructures have been designed as signal amplifiers to construct electrochemical immunosensors.[41,42] For instance, Wang *et al.*[43] prepared horseradish peroxidase (HRP)/gold nanoparticles (Au) on $TiO_2$/graphene as signal amplifier for constructing an immunosensor of carcinoembryonic antigen based on the electrocatalytic current of HRP/$H_2O_2$ toward hydroquinone reduction. In addition, similar ways for signal amplification based on RGO and electrocatalysis of HRP were also developed for squamous cell carcinoma antigen,[44] prostate specific antigen[45] and cardiac troponin I.[46] Obviously, the preparation methods and sensing mechanisms of these signal amplifiers are relatively complex.

Herein, carboxyl $Ti_3C_2T_x$ MXene (C-$Ti_3C_2T_x$ MXene) and gold/RGO/rhodamine b (Au/RGO/RhB) nanostructures were prepared respectively as sensing platform and signal amplifier. By functionalizing $Ti_3C_2T_x$ MXene with carboxyl, the formed C-$Ti_3C_2T_x$ MXene can immobilize LM primary antibody (PAb) *via* a simple amidation reaction to capture LM targets. As for Au/RGO/RhB, RhB was non-covalently functionalized on the Au/RGO surface *via* π–π stacking to be used as a desirable probe since it exhibits sensitive electrochemical oxidation current, and the secondary antibody (SAb) was assembled on the Au surface. On the basis of the above principle, a new sandwich-like electrochemical immunosensing platform was constructed for detecting LM (Scheme 1) coupled with an excellent sensing performance under the optimized conditions.

## 2. Experimental section

### 2.1 Preparation of C-$Ti_3C_2T_x$ MXene

$Ti_3C_2T_x$ MXene was first prepared by etching the aluminum layer from $Ti_3AlC_2$ according to a previous method.[47] Briefly, 1.0 g $Ti_3AlC_2$ powder was added slowly to 20.0 mL HF solution under stirring at ~35 °C and maintained for ~24 h. After centrifuging, washing and drying of the precipitate, $Ti_3C_2T_x$ MXene was obtained successfully.

Next, C-$Ti_3C_2T_x$ MXene was prepared according to a previous work with some modifications.[48] In brief, 0.16 g 4-aminobenzoic acid and 0.14 g sodium hydroxide were first added to 50.0 mL water (~2 °C), and then 0.26 g sodium nitrite (7.6 mM) was added slowly. Subsequently, 6.0 mL HCl solution was quickly added to this solution under stirring and kept for ~40 min. Then, the desired diazonium salt solution was added to 20.0 mL of $Ti_3C_2T_x$ solution (5.0 mg $mL^{-1}$) and allowed to stir for ~5 hours. Finally, the solution was centrifuged, washed and dried to obtain the C-$Ti_3C_2T_x$ MXene product.

### 2.2 Preparation of Au/RGO/RhB

Before the preparation of Au/RGO/RhB, Au/RGO was prepared *via* a common method.[49,50] For preparing RhB/Au/RGO, 20.0 mL of Au/RGO dispersion (0.5 mg $mL^{-1}$) was mixed with 20.0 mL of RhB solution (0.25 mg $mL^{-1}$) and stirred continuously for ~30 min. Owing to the π–π stacking between RhB and RGO, the RhB molecules were functionalized non-covalently on the RGO surface. After centrifugation, rinsing and vacuum-drying, the Au/RGO/RhB product was obtained successfully.

### 2.3 Construction of the sandwich-like immunosensor

SAb (30.0 μL) was added to 4.0 mL Au/RGO/RhB dispersion (0.5 mg mL) and incubated at room temperature for ~2 hour to assemble SAb on Au surface, forming SAb-Au/RGO/RhB. Next, 10.0 μL C-$Ti_3C_2T_x$ MXene suspension of (0.5 mg $mL^{-1}$) was dropped onto a cleaned glassy carbon electrode (GCE) and a 1 : 1 mixture of 1-ethyl-3-[3-dimethylaminopropyl] carbodiimide hydrochloride (0.1 M) with *N*-hydroxysuccinimide mixture (0.2 M) was used to activate the carboxyl group for 30 min. Sequentially, PAb solution (8.0 μL) was dropped and assembled on the activated C-$Ti_3C_2T_x$ MXene/GCE surface, denoting the formed electrode as PAb/$Ti_3C_2T_x$ MXene/GCE. Phosphate buffer solution (PBS) was then used to rinse PAb/$Ti_3C_2T_x$ MXene/GCE to remove the unbound PAb, and 4.0 μL BSA (0.1 g $mL^{-1}$) was used to prevent nonspecific adsorption by incubating PAb/$Ti_3C_2T_x$ MXene/GCE with BSA to form BSA/PAb/$Ti_3C_2T_x$ MXene/GCE. For LA sensing, the constructed BSA/PAb/$Ti_3C_2T_x$ MXene/GCE reacted with LM at different concentrations and dipped in PBS to eliminate nonspecific LM cell.

 

Finally, LM/BSA/PAb/$Ti_3C_2T_x$ MXene/GCE was combined with SAb-Au/RGO/RhB to produce a sandwich-like structure, which was then measured by an electrochemical method.

## 3. Results and discussion

### 3.1 Characterization of C-$Ti_3C_2T_x$ MXene and Au/RGO/RhB

Fig. 1 shows the scanning electron microscopy (SEM) images of $Ti_3AlC_2$ MAX phase precursor and $Ti_3C_2T_x$ MXene. It is noted that the pristine $Ti_3AlC_2$ particles exhibit densely aligned layered structures with smooth surface (Fig. 1A). After etching with HF, the produced $Ti_3C_2T_x$ layered nanostructures become very evident and exhibit loosely packed accordion-like morphology compared to the initial $Ti_3AlC_2$ sample (Fig. 1B).

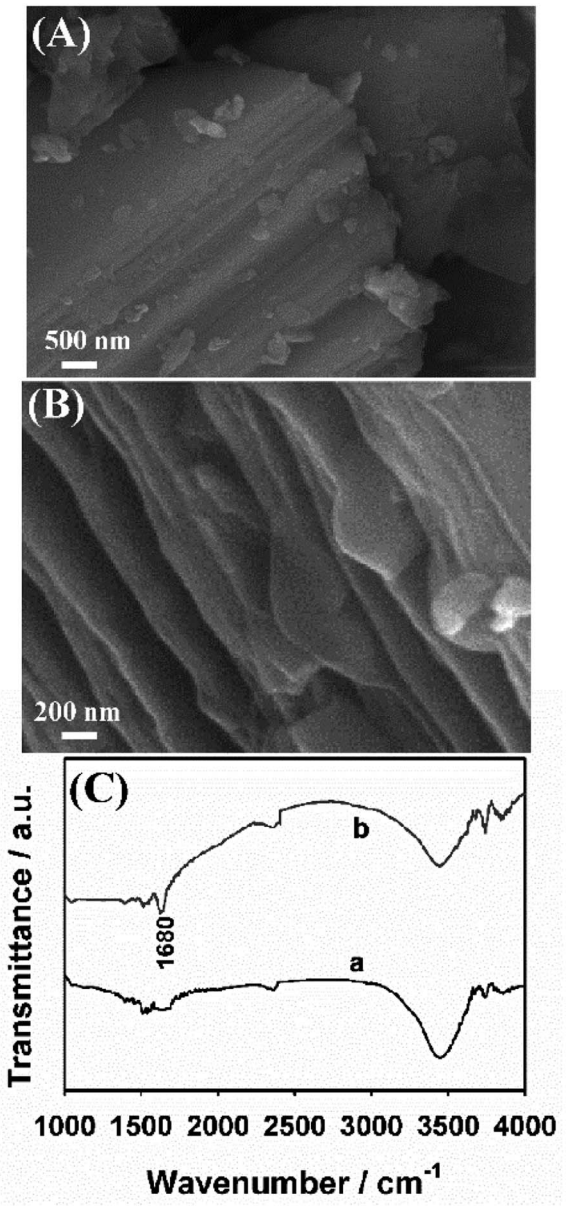


Fig. 1 The SEM images of (A) $Ti_3AlC_2$ and (B) $Ti_3C_2T_x$; (C) FT-IR spectra of $Ti_3C_2T_x$ MXene (a) and C-$Ti_3C_2T_x$ MXene (b).

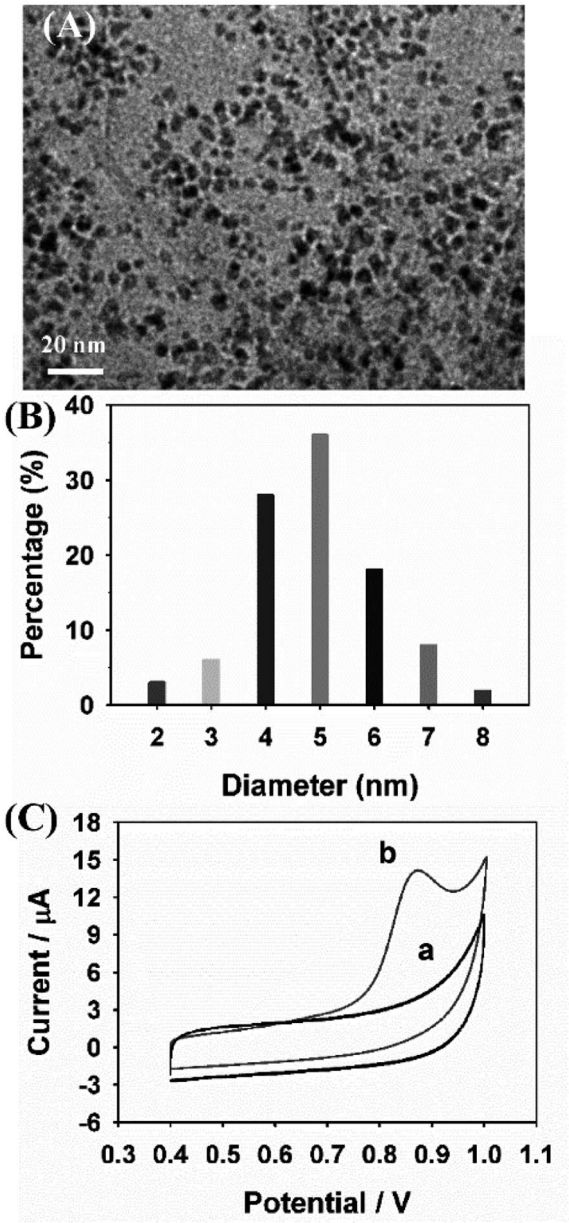


Fig. 2 (A) The TEM image of Au/RGO hybrid, (B) the particle size distribution of AuNPs, and (C) the CV responses of Au/RGO (a) and Au/RGO/RhB (b).

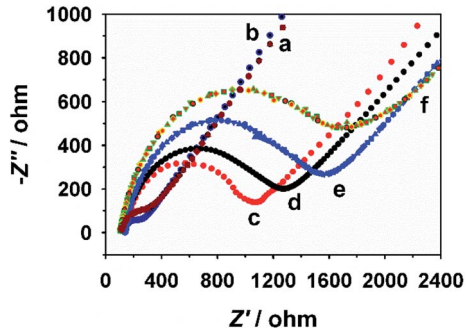


Fig. 3 The EIS plots of GCE (a), C-$Ti_3C_2T_x$ MXene/GCE (b), PAb/$Ti_3C_2T_x$ MXene/GCE (c), BSA/PAb/$Ti_3C_2T_x$ MXene/GCE (d), LM/BSA/PAb/$Ti_3C_2T_x$ MXene/GCE (e), and SAb-Au/RGO/RhB/LM/BSA/PAb/$Ti_3C_2T_x$ MXene/GCE (f).

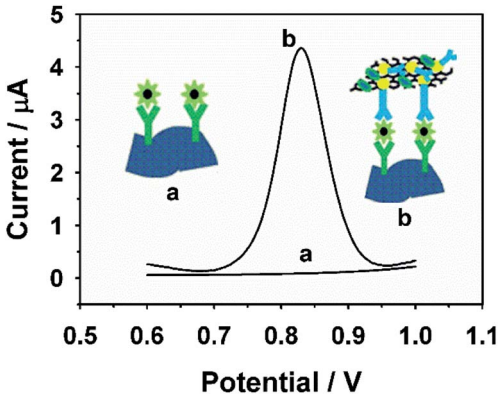


Fig. 4 The DPV response of LM/BSA/PAb/$Ti_3C_2T_x$ MXene/GCE (a) and SAb-Au/RGO/RhB/LM/BSA/PAb/$Ti_3C_2T_x$ MXene/GCE (b) in 0.1 M PBS.

Fourier transform infrared (FT-IR) spectroscopy was used to characterize the formation of C-$Ti_3C_2T_x$ MXene (Fig. 1C). Compared with $Ti_3C_2T_x$ MXene, C-$Ti_3C_2T_x$ MXene possesses a typical and strong characteristic peak of carboxyl presented at ~1680 $cm^{-1}$.

Fig. 2A shows the transmission electron microscopy (TEM) images of Au/RGO hybrids; it was found that Au nanoparticles were distributed uniformly on the RGO surface with an average diameter of ~5.0 nm (Fig. 2B), and ICP-AES demonstrated that the content of Au is ~5.7%. The abundant and uniform Au present on the Au/RGO surface is very important to assemble SAb and improve the sensing capability. The functionalization of RhB towards Au/RGO can be easily demonstrated by cyclic voltammetry (CV). As shown in Fig. 2C, there is no peak current present between 0.4 and 1.0 V, while Au/RGO/RhB shows a remarkable oxidation peak current at ~0.87 V since RhB is an electroactive molecule.

### 3.2 Electrochemical evaluation of the sandwich-like immunosensor

Firstly, electrochemical impedance spectroscopy (EIS) was introduced to evaluate the procedures in constructing the immunosensing platform, which was performed in a 5.0 mM $[Fe(CN)_6]^{3-/4-}$solution (Fig. 3). Generally, biomolecules including antibody, LM cells and BSA are non-conductive and could restrain electron channel to increase the $R_{CT}$ values. As shown in Fig. 3, the charge-transfer resistance ($R_{CT}$) at C-$Ti_3C_2T_x$ MXene/GCE is smaller than that of bare GCE due to the high conductivity of $Ti_3C_2T_x$ MXene. When C-$Ti_3C_2T_x$ MXene/GCE was assembled successively with PAB, LM and SAb-Au/RGO/RhB/LM, the $R_{CT}$ values at PAb/$Ti_3C_2T_x$ MXene/GCE, BSA/PAb/$Ti_3C_2T_x$ MXene/GCE, LM/BSA/PAb/$Ti_3C_2T_x$ MXene/GCE and SAb-Au/RGO/RhB/LM/BSA/PAb/$Ti_3C_2T_x$ MXene/GCE in turn show an increase. These results indicate that the developed immunosensing layers were fabricated successfully.

The feasibility of the proposed immunosensor was studied by differential pulse voltammetry (DPV) technique. As shown in Fig. 4 (LM concentration, $10^6$ CFU $mL^{-1}$), there is no peak current observed at LM/BSA/PAb/$Ti_3C_2T_x$ MXene/GCE in 0.1 M

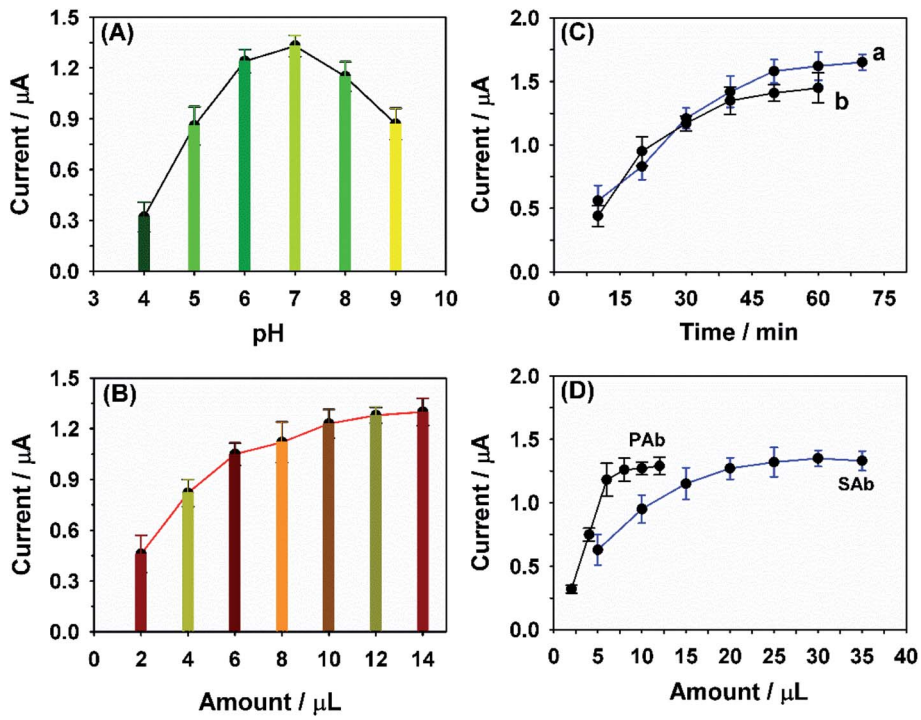


Fig. 5 Influence of the (A) pH value of PBS; (B) amount of $Ti_3C_2T_x$ MXene; (C) reaction time of LM with BSA/PAb/$Ti_3C_2T_x$ MXene/GCE (a) and LM/BSA/PAb/$Ti_3C_2T_x$ MXene with SAb-Au/RGO/RhB (b); (D) amount of PAb and SAb. The specific values of the error bar for (A), (B), (C) and (D) are 0.1 ± 0.03, 0.17 ± 0.04, 0.09 ± 0.03 and 0.08 ± 0.03, respectively.

 

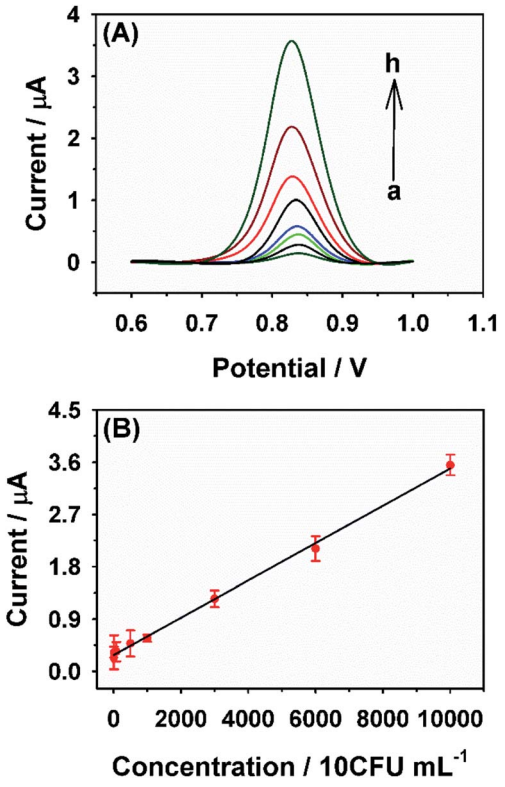


Fig. 6 (A) The DPV responses of LM with various concentrations in 0.1 M PBS (from a to h: 10, 100, 800, $5 \times 10^3$, $10^4$, $3 \times 10^4$, $6 \times 10^4$ and $10^5$ CFU $mL^{-1}$) based on the developed immunosensor; (B) the calibration plot of LM. The specific value of the error bar for (B) is 0.18 ± 0.06.

PBS (pH 7.0). As for SAb-Au/RGO/RhB/LM/BSA/PAb/$Ti_3C_2T_x$ MXene/GCE, it exhibits an obvious peak current of RhB due to the capture of SAb-Au/RGO/RhB resulting from the antigen–antibody reaction, indicating that the developed immunosensing method is feasible for LM detection. In order to achieve high sensitivity in sensing LM, a series of controlled experiments were performed.

In general, excessive acidity or alkalinity could enable various proteins to become unstable, thus the effect from PBS needs to be evaluated. As shown in Fig. 5A, the DPV peak currents of SAb-Au/RGO/RhB/LM/BSA/PAb/$Ti_3C_2T_x$ MXene/GCE increase along with the increase in pH value from 4.0, and the maximum peak current presents at pH value of 7.0, thus PBS with the value of 7.0 was selected for all the experiments. Meanwhile, the C-$Ti_3C_2T_x$ MXene amount coated on the GCE surface is important for the sensing capability, and Fig. 5B shows that the peak currents of RhB increase along with the increase in the amount from 2.0 to 10.0 μL. When the used amount exceeds 10.0 μL, there is little change in the RhB peak currents, indicating that 10.0 μL C-$Ti_3C_2T_x$ MXene dispersion was enough. Furthermore, the incubation time between LM with different antibodies was studied. As shown in Fig. 5C, the studies demonstrated that the optimum length for reacting LM with PAb was 50 min, while the time for reacting LM with SAb was 40 min. The concentration of LM used for the controlled experiments was $3 \times 10^4$ CFU $mL^{-1}$. In addition, the amounts of PAb and SAb used in the construction of the immunosensor were also studied, and it can be observed from Fig. 5D that the best amounts of PAb and SAb were 8.0 and 30.0 μL, respectively.

Under the above optimized controlled conditions, the quantitative sensing of LM was performed using DPV based on the proposed SAb-Au/RGO/RhB/LM/BSA/PAb/$Ti_3C_2T_x$ MXene sandwich-like immunosensor. From Fig. 6, it is observed that the peak currents of RhB probe linearly increase along with the increase in concentration of LM from 10 and $10^5$ CFU $mL^{-1}$. The linear equation expression is $I_p$ (μA) = 0.281 + 0.003$C$ (CFU $mL^{-1}$) ($R$ = 0.998) and limit of detection (LOD) is calculated to be 2 ± 0.3 CFU $mL^{-1}$ (S/N, 3). Compared with most previous works, the present work exhibits better sensing performance including linearity range (LR) and LOD (Table 1); this can attributed mainly to the desirable properties of $Ti_3C_2T_x$ MXene (large surface area and conductivity) and the signal amplification capacity of Au/RGO/RhB.

### 3.3 Specificity, reproducibility and stability of the developed immunosensing platform

For further evaluating the specificity of the developed sandwich-like immunosensor, the response signals of RhB were studied through selecting other pathogens other than LM. As exhibited in Fig. 7A, the obtained results revealed a significant peak current of RhB observed only from LM ($10^4$ CFU $mL^{-1}$); as for the other pathogens including *Escherichia coli* (Es), *Vibrio parahaemolyticus* (Vp), *Shigella* (Sh), *Salmonella enteritidis* (Se) and *Staphylococcus aureus* (Sac) coupled with a high concentration ($5 \times 10^4$ CFU $mL^{-1}$), the presented peak currents of RhB are nearly negligible, demonstrating that the developed sandwich-like immunosensor offers excellent specificity for detecting LM.

Next, for evaluating the reproducibility of the immunosensor, the electrochemical responses of 8 fabricated sensors were measured parallelly (Fig. 7B), and the results display that

Table 1 Comparison of various immunosensing platforms with the present method for LM

| Electrodes | Assay label | Measuring method | Linear range/CFU $mL^{-1}$ | LOD/CFU $mL^{-1}$ | Reference |
|---|---|---|---|---|---|
| Gold electrode | HRP | Amperometry | $10^2$ to $10^6$ | $10^2$ | 6 |
| Interdigitated array microelectrode | Urease | EIS | $1.9 \times 10^3$ to $1.9 \times 10^6$ | $1.6 \times 10^3$ | 51 |
| $TiO_2$ nanowire bundle gold microelectrode | Label-free | EIS | — | $10^2$ | 52 |
| Au NPs/screen-printed carbon electrode | HRP | Amperometry | $2.25 \times 10$ to $2.25 \times 10^5$ | $2.25 \times 10^2$ | 53 |
| CNT fibers electrode | HRP | Cyclic voltammetry | $10^2$ to $10^5$ | $1.07 \times 10^2$ | 54 |
| C-$Ti_3C_2T_x$ MXene/GCE | RhB | DPV | 10 to $10^5$ | 2 ± 0.3 | This work |

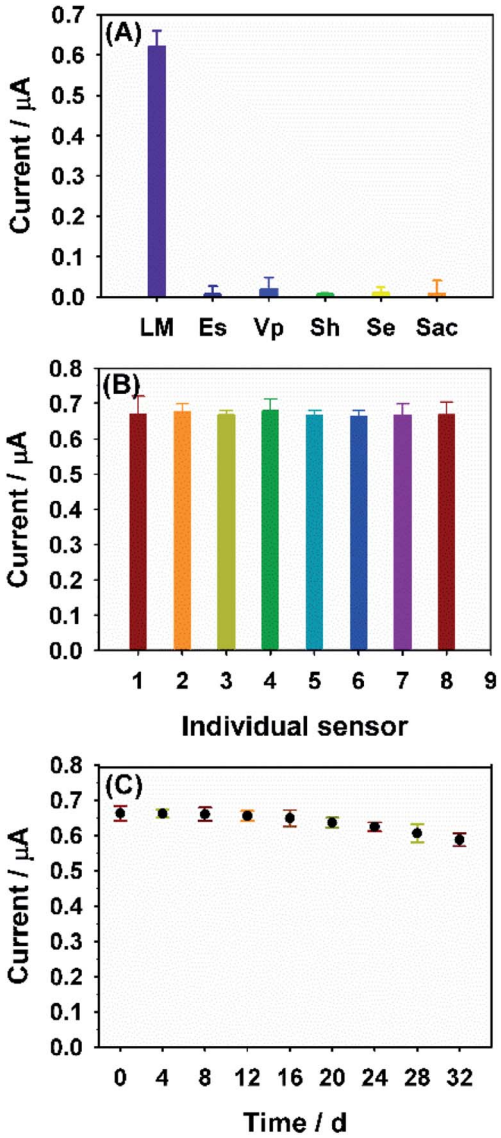


Fig. 7 (A) Specificity, (B) reproducibility and (C) stability for LM detection based on the constructed sandwich-like immunosensor. The specific values of the error bar for (A), (B) and (C) are 0.02 ± 0.006, 0.03 ± 0.005 and 0.02 ± 0.004, respectively.

the relative standard deviation value from their current response was 4.36%. Furthermore, in order to study the immunosensor stability, the modified electrodes and SAb-Au/RGO/RhB were stored at 4 °C for further use; the research results showed almost no decrease in the current response (~5.32%) after storing for 32 days (Fig. 7C). These results reveal that the proposed immunosensor possesses satisfactory reproducibility and good stability.

## 4. Conclusion

By preparing C-$Ti_3C_2T_x$ MXene and Au/RGO/RhB respectively as the sensing platform and signal amplifier, a new sandwich-like electrochemical immunosensing platform was constructed herein for the sensitive determination of LM. Owing to the superior properties of $Ti_3C_2T_x$ MXene and Au/RGO/RhB, the developed SAb-Au/RGO/RhB/LM/BSA/PAb/$Ti_3C_2T_x$ MXene sandwich-like immunosensor possesses wider LR and lower LOD than most previous works for detecting LM; thus it is believed that this sensor has great potential for application in LM analysis. Furthermore, through selecting other suitable antibodies other than LM antibodies, the sandwich-like immunosensor based on the prepared C-$Ti_3C_2T_x$ MXene and Au/RGO/RhB shows broad application prospects for other targets.

## Conflicts of interest

There are no conflicts to declare.

## Acknowledgements

This work was financially supported in part by Research Project of Military Logistics of PLA of China (No. CLB20J024), Foreign cooperation projects of Fujian Natural Science Foundation (No. 2019I0025), National Natural Science Foundation of China (No. 81772848), Joint Funds for the Innovation of Science and Technology from Fujian Province (No. 2017Y9127), and Fund from the 900th Hospital of Joint Logistics Support Force (No. 2020Q01, 2020Q06, 2020Z15, and 2020L17).

## References

1 N. F. D. Silva, M. M. P. S. Neves, J. M. C. S. Magalhães, C. Freire and C. Delerue-Matos, *Trends Food Sci. Technol.*, 2020, **99**, 621–633.
2 J. Ding, J. Lei, X. Ma, J. Gong and W. Qin, *Anal. Chem.*, 2014, **86**, 9412–9416.
3 D. Patel, Y. Zhou and R. P. Ramasamy, *J. Electrochem. Soc.*, 2021, **168**, 057523.
4 X. Qi, Z. Wang, R. Lu, J. Liu, Y. Li and Y. Chen, *Food Chem.*, 2021, **338**, 127837.
5 S. Eissa and M. Zourob, *Microchim. Acta*, 2020, **187**, 486.
6 C. Cheng, Y. Peng, J. Bai, X. Zhang, Y. Liu, X. Fan, B. Ning and Z. Gao, *Sens. Actuators, B*, 2014, **190**, 900–906.
7 Q. Chen, J. Lin, C. Gan, Y. Wang, D. Wang, Y. Xiong, W. Lai, Y. Li and M. Wang, *Biosens. Bioelectron.*, 2015, **74**, 504–511.
8 B. Giménez, N. Graiver, L. Giannuzzi and N. Zaritzky, *Food Control*, 2021, **121**, 107602.
9 B. B. Tasbasi, B. C. Guner, M. Sudagidan, S. Ucak, M. Kavruk and V. C. Ozalp, *Anal. Biochem.*, 2019, **587**, 113449.
10 S. Wachiralurpan, K. Chansiri and P. A. Lieberzeit, *Sens. Actuators, B*, 2020, **308**, 127678.
11 Y. Zhao, S. Bu, C. Wang, C. Ma, Z. Li, W. Zhang and J. Wan, *Anal. Lett.*, 2021, **54**, 1603–1615.
12 J. Riu and B. Giussani, *Trac. Trends Anal. Chem.*, 2020, **126**, 115863.
13 X. Niu, W. Zheng, C. Yin, W. Weng, G. Li, W. Sun and Y. Men, *J. Electroanal. Chem.*, 2017, **806**, 116–122.
14 A. Liu, L. Shen, Z. Zeng, M. Sun, Y. Liu, S. Liu, C. Li and X. Wang, *Food Anal. Methods*, 2018, **11**, 215–223.

 

15 N. F. D. Silva, M. M. P. S. Neves, J. M. C. S. Magalhães, C. Freire and C. Delerue-Matos, *Talanta*, 2020, **216**, 120976.
16 Q. Guo, X. Zhang, F. Zhao, Q. Song, G. Su, Y. Tan, Q. Tao, T. Zhou, Y. Yu, Z. Zhou and C. Lu, *ACS Nano*, 2020, **14**, 2788–2797.
17 Y. Li, H. Shao, Z. Lin, J. Lu, L. Liu, B. Duployer, P. O. Å. Persson, P. Eklund, L. Hultman, M. Li, K. Chen, X.-H. Zha, S. Du, P. Rozier, Z. Chai, E. Raymundo-Piñero, P.-L. Taberna, P. Simon and Q. Huang, *Nat. Mater.*, 2020, **19**, 894–899.
18 M. Zhou, S. Ning, J. Liu, G. I. N. Waterhouse, L. Li, J. Dong and S. Ai, *Anal. Lett.*, 2021, **54**, 1769–1782.
19 J. Chen, P. Tong, L. Huang, Z. Yu and D. Tang, *Electrochim. Acta*, 2019, **319**, 375–381.
20 G. Cai, Z. Yu, P. Tong and D. Tang, *Nanoscale*, 2019, **11**, 15659–15667.
21 L. Wu, X. Lu, Dhanjai, Z.-S. Wu, Y. Dong, X. Wang, S. Zheng and J. Chen, *Biosens. Bioelectron.*, 2018, **107**, 69–75.
22 P. K. Kalambate, Dhanjai, A. Sinha, Y. Li, Y. Shen and Y. Huang, *Microchim. Acta*, 2020, **187**, 402.
23 Y. Xie, F. Gao, X. Tu, X. Ma, Q. Xu, R. Dai, X. Huang, Y. Yu and L. Lu, *J. Electrochem. Soc.*, 2019, **166**, B1673–B1680.
24 Y. Yi, D. Zhang, Y. Ma, X. Wu and G. Zhu, *Anal. Chem.*, 2019, **91**, 2908–2915.
25 X. Tu, F. Gao, X. Ma, J. Zou, Y. Yu, M. Li, F. Qu, X. Huang and L. Lu, *J. Hazard. Mater.*, 2020, **396**, 122776.
26 H. Zhang, Z. Wang, F. Wang, Y. Zhang, H. Wang and Y. Liu, *Anal. Chem.*, 2020, **92**, 5546–5553.
27 P. K. Kalambate, N. S. Gadhari, X. Li, Z. Rao, S. T. Navale, Y. Shen, V. R. Patil and Y. Huang, *Trac. Trends Anal. Chem.*, 2019, **120**, 115643.
28 Y. Yi, Y. Ma, F. Ai, Y. Xia, H. Lin and G. Zhu, *Chem. Commun.*, 2021, **57**, 7790–7793.
29 Y. Xia, Y. Ma, Y. Wu, Y. Yi, H. Lin and G. Zhu, *Microchim. Acta*, 2021, **188**, 1–9.
30 Y. Xia, Y. Zhao, F. Ai, Y. Yi, T. Liu, H. Lin and G. Zhu, *J. Hazard Mater.*, 2021, 127974.
31 R. Zeng, W. Wang, M. Chen, Q. Wan, C. Wang, D. Knopp and D. Tang, *Nano Energy*, 2021, **82**, 105711.
32 R. Zeng, Z. Luo, L. Zhang and D. Tang, *Anal. Chem.*, 2018, **90**, 12299–12306.
33 Y. Yao, L. Lan, X. Liu, Y. Ying and J. Ping, *Biosens. Bioelectron.*, 2020, **148**, 111799.
34 M. Mohammadniaei, A. Koyappayil, Y. Sun, J. Min and M.-H. Lee, *Biosens. Bioelectron.*, 2020, **159**, 112208.
35 Y. Cai, J. Shen, G. Ge, Y. Zhang, W. Jin, W. Huang, J. Shao, J. Yang and X. Dong, *ACS Nano*, 2018, **12**, 56–62.
36 D. Huang, Y. Wu, F. Ai, X. Zhou and G. Zhu, *Sens. Actuators, B*, 2021, **342**, 130074.
37 L. Jothi, S. K. Jaganathan and G. Nageswaran, *Mater. Chem. Phys.*, 2020, **242**, 122514.
38 P. Zhao, M. Ni, Y. Xu, C. Wang, C. Chen, X. Zhang, C. Li, Y. Xie and J. Fei, *Sens. Actuators, B*, 2019, **299**, 126997.
39 K. Kunpatee, P. Chamsai, E. Mehmeti, D. M. Stankovic, A. Ortner, K. Kalcher and A. Samphao, *J. Electroanal. Chem.*, 2019, **855**, 113630.
40 R. Zhang, C. Zhang, F. Zheng, X. Li, C.-L. Sun and W. Chen, *Carbon*, 2018, **126**, 328–337.
41 S. Lv, K. Zhang, Y. Zeng and D. Tang, *Anal. Chem.*, 2018, **90**, 7086–7093.
42 Q. Zhou, Y. Lin, K. Zhang, M. Li and D. Tang, *Biosens. Bioelectron.*, 2018, **101**, 146–152.
43 Y. Chen, Y. Li, D. Deng, H. He, X. Yan, Z. Wang, C. Fan and L. Luo, *Biosens. Bioelectron.*, 2018, **102**, 301–306.
44 Y. Liu, H. Ma, J. Gao, D. Wu, X. Ren, T. Yan, X. Pang and Q. Wei, *Biosens. Bioelectron.*, 2016, **79**, 71–78.
45 M. Li, P. Wang, F. Li, Q. Chu, Y. Li and Y. Dong, *Biosens. Bioelectron.*, 2017, **87**, 752–759.
46 H. Lv, X. Zhang, Y. Li, Y. Ren, C. Zhang, P. Wang, Z. Xu, X. Li, Z. Chen and Y. Dong, *Microchim. Acta*, 2019, **186**, 1–10.
47 H. Wu, M. Almalki, X. Xu, Y. Lei, F. Ming, A. Mallick, V. Roddatis, S. Lopatin, O. Shekhah, M. Eddaoudi and H. N. Alshareef, *J. Am. Chem. Soc.*, 2019, **141**, 20037–20042.
48 P. Zhang, L. Wang, K. Du, S. Wang, Z. Huang, L. Yuan, Z. Li, H. Wang, L. Zheng and Z. Chai, *J. Hazard Mater.*, 2020, **396**, 122731.
49 F. Cui and X. Zhang, *J. Electroanal. Chem.*, 2012, **669**, 35–41.
50 G. Goncalves, P. A. A. P. Marques, C. M. Granadeiro, H. I. S. Nogueira, M. K. Singh and J. Grácio, *Chem. Mater.*, 2009, **21**, 4796–4802.
51 D. Wang, Q. Chen, H. Huo, S. Bai, G. Cai, W. Lai and J. Lin, *Food Control*, 2017, **73**, 555–561.
52 R. Wang, C. Ruan, D. Kanayeva, K. Lassiter and Y. Li, *Nano Lett.*, 2008, **8**, 2625–2631.
53 D. Davis, X. Guo, L. Musavi, C. S. Lin, S. H. Chen and V. C. H. Wu, *Ind. Biotechnol.*, 2013, **9**, 31–36.
54 Y. Lu, Y. Liu, Y. Zhao, W. Li, L. Qiu and L. Li, *J. Nanomater.*, 2016, **2016**, 16.